PHYSICAL REVIEW X **13**, 041025 (2023)

Simultaneous Enantiomer-Resolved Ramsey Spectroscopy Scheme for Chiral Molecules

Itay Erez,[1,2] Eliana Ruth Wallach,[1,2] and Yuval Shagam[1,*]
[1]*Schulich Faculty of Chemistry, Solid State Institute and The Helen Diller Quantum Center,*
Technion-Israel Institute of Technology, Haifa, 3200003, Israel
[2]*Physics Department, Technion-Israel Institute of Technology, Haifa, 3200003, Israel*

(Received 7 June 2022; accepted 22 September 2023; published 6 November 2023)

Chiral molecules provide an ideal test platform to search for symmetry breaking in nature, due to the perfect parity symmetry of their left- and right-handed enantiomers under the electromagnetic interaction. This high degree of symmetry drives efforts to probe the two enantiomers individually after they have been chemically separated, but this allows external effects to influence the measurement, ultimately harming the precision. In particular, the complexity of such polyatomic molecules makes them difficult to control and detect precisely. Employing a more symmetrical measurement procedure can improve the experiment fidelity and alleviate issues associated with molecular complexity. To this end, we theoretically introduce a scheme to perform Ramsey spectroscopy on a racemic mixture of chiral molecules, simultaneously extracting the transition frequencies of the two enantiomers. By taking the difference between the enantiospecific frequencies, we isolate parity violating effects such as the weak force, which is predicted to break the symmetry between enantiomers. To perform the scheme, we design a pulse sequence that creates enantiospecific superpositions in a three-level system using the enantiomer-dependent sign of the electric-dipole moment components' triple product. A delayed second pulse sequence completes the Ramsey interrogation sequence, enabling readout of the phase evolution for each enantiomer's transition through a separate quantum state. Our technique overcomes the need to alternate between enantiopure samples to measure parity violation, and is applicable to both charged and neutral molecular species. We describe the advantages of the proposed method for precision metrology.

DOI: 10.1103/PhysRevX.13.041025 Subject Areas: Atomic and Molecular Physics

I. INTRODUCTION

The first observation of parity violation (PV) was reported nearly 70 years ago in the decay of ^{60}Co [1], shortly after parity conservation by the weak interaction was questioned [2]. The weak force also has nonradioactive components known as neutral currents, which violate parity symmetry as detected in atomic transitions [3–6]. Thus far, PV has not been observed in chiral molecules, which are the prototypical example of mirror-image symmetry in nature. Hund originally modeled chiral molecules as a symmetric double-well potential [7], but the addition of PV creates an asymmetric double well as shown in Fig. 1(a) with an exaggerated skew [8]. The resulting vibrational transition frequencies of each enantiomer are shifted by $\pm\Delta_{\mathrm{PV}}^{\mathrm{vib}}$ [9,10] due to the different anharmonicity in the $\mathcal{S}$ and $\mathcal{R}$ wells. Observation of PV in chiral molecules would confirm the prediction that the weak force is responsible for eliminating the so-called inter-enantiomer tunneling [8]. It has even been hypothesized that this symmetry breaking seeds the chiral excess exhibited in the chemistry of life, although this remains controversial [8,11–15]. Measurement of PV also has prospects beyond the Standard Model [16] such as in dark matter searches [17].

The challenge of measuring $\Delta_{\mathrm{PV}}^{\mathrm{vib}}$ lies in its tiny magnitude, where estimations for organic chiral molecules such as CHBrClF are smaller than 10 mHz or a 10^{-16} shift relative to the vibrational transition [10]. However, calculations predict that $\Delta_{\mathrm{PV}}^{\mathrm{vib}}$ can be enhanced by 2 orders of magnitude for electronically excited and ionized states, due to the reduced cancellation of PV contributions from different orbitals [15,18]. Indeed for CHDBrI^{+} the vibrational parity violation energy shift is found to be $\sim$1 Hz or a 10^{-14} relative shift [19,20]. An alternative approach to increase the effect utilizes substitution of heavy metal nuclei in the molecule [21–25]. In NUHFI, for example, $\Delta_{\mathrm{PV}}^{\mathrm{vib}}$ is calculated to rise to the order of 10 Hz or a 10^{-13} relative shift [25].

Multiple techniques have been used and proposed to measure PV in chiral molecules including using parity selection rules [26], Fourier transform infrared spectroscopy [27–29], microwave spectroscopy [30], vibrational

---

[*] yush@technion.ac.il

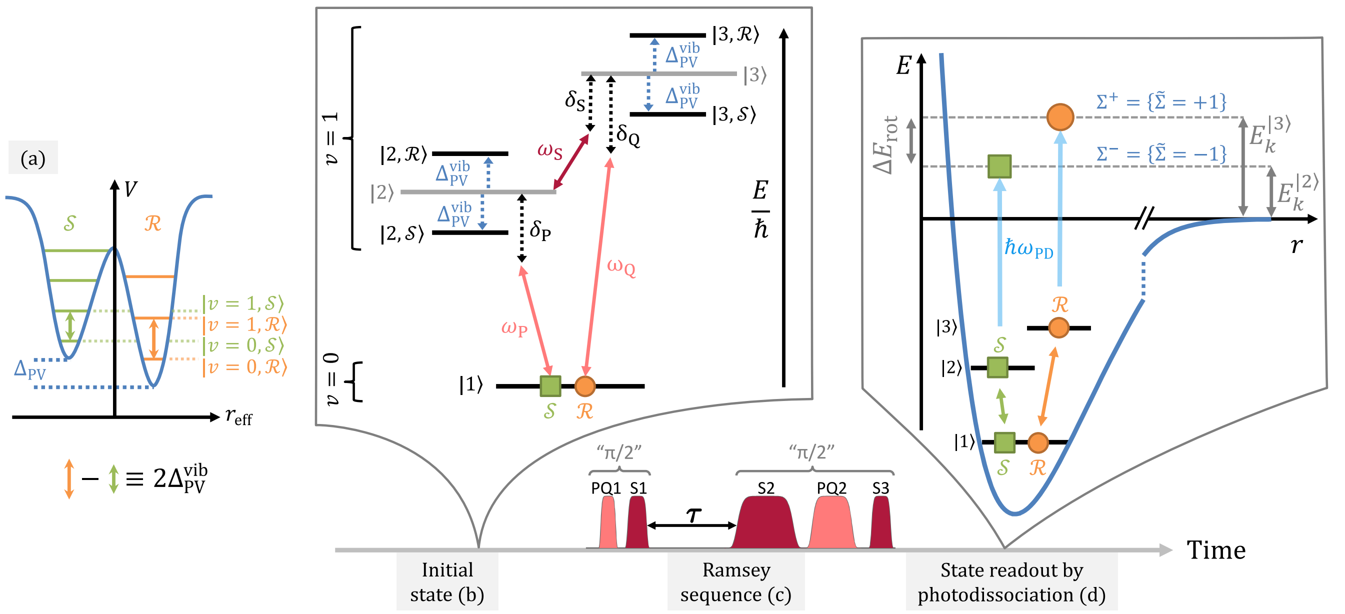

FIG. 1. Schematic outline of the simultaneous Ramsey sequence to measure the vibrational frequency shift $2\Delta_{\mathrm{PV}}^{\mathrm{vib}}$ in a racemic sample. The chiral molecule is described by an asymmetric double-well potential when including PV from weak interaction, which is exaggerated for emphasis (a). The $\mathcal{R}$ well is arbitrarily chosen to be deeper than the $\mathcal{S}$ well. When considering the ground vibrational level $|1\rangle$ and two rotational states $|2\rangle$ and $|3\rangle$ in the first excited vibrational level, the slight difference in frequencies of the two wells leads to an offset between the transitions of $\mathcal{S}$ and $\mathcal{R}$ molecules, denoted $2\Delta_{\mathrm{PV}}^{\mathrm{vib}}$ (b). The transitions between the three states are labeled P (pink), Q (pink), and S (dark red) and are driven by fields with the frequencies $\omega_{\mathrm{P}}, \omega_{\mathrm{Q}}, \omega_{\mathrm{S}}$ that are detuned by $\delta_{\mathrm{P}}, \delta_{\mathrm{Q}}, \delta_{\mathrm{S}}$ from resonance, respectively (b). The fields are mutually orthogonally polarized. The molecules initially populate $|1\rangle$ and after the Ramsey sequence, which is composed of multiple individual pulses with varying application durations [as plotted in (c); see Sec. III D], part of the population of $\mathcal{S}$ is transferred to $|2\rangle$ and part of $\mathcal{R}$ to $|3\rangle$ for the case $\tilde{\Phi}=-1$ which is depicted here. The populations in $|2\rangle$ and $|3\rangle$ oscillate depending on the free evolution time τ according to each enantiomer's detuning. Resolved readout of states $|2\rangle$ and $|3\rangle$ to characterize the two Ramsey fringes is possible by photodissociation (PD), separating the two states by the kinetic energy of the photofragments (d).

Ramsey spectroscopy [31], NMR spectroscopy [32], and matter-wave interferometry [33]. In most of these techniques, the ability to synthesize enantiomer-enriched samples has been described as a key requirement [30,34,35]. However, realizing this requirement is difficult for the molecules that are particularly appealing for PV measurement.

An alternative to comparing enantioenriched samples to search for PV is to probe an enantioenriched signal in an experiment where the initial sample is mixed. Multiple methods exist with varying degrees of detection enantioselectiveness including circular dichroism [36] and Coulomb explosion [37]. One scheme, known as three-wave mixing (3WM) [38], has particularly excellent prospects for efficient enrichment by separating enantiomers into different quantum states [39–47]. Its principles form the foundation of our work. The scheme has been demonstrated to excite a sample of $\mathcal{S}$ and $\mathcal{R}$ molecules from an initial state $|1\rangle$ to either state $|2\rangle$ or $|3\rangle$ using the enantiomer-specific sign of the triple product of the transition dipole moment components.

Here we propose a fully differential scheme that leverages racemic enantiomer mixtures to directly extract the PV signature. Instead of comparing transitions in separate enantiopure samples, we theoretically design an identical procedure for both enantiomers, which combines Ramsey spectroscopy and 3WM, to simultaneously measure two transition frequencies in a racemic sample. This trait implies support for common-mode noise rejection for the difference between the transitions, with the statistical sensitivity likely approaching the standard quantum limit (SQL) as demonstrated in Ref. [48]. This makes our scheme particularly appealing for precision measurement. Finally, we introduce a framework of experimental switches that isolate the PV contribution. We discuss the benefits of our procedure, which is embedded within the 3WM, three-state framework, over the sequential concatenation of standard, two-state, vibrational Ramsey spectroscopy followed by a microwave 3WM step.

II. BACKGROUND

In this proposal, we combine ideas and methods that come from precision metrology and microwave 3WM spectroscopy. These include Ramsey spectroscopy, enantiomer-specific state transfer (ESST), and differential measurement. We briefly review these in this section.

A. Ramsey interferometry

Ramsey interferometry is a common precision spectroscopy method that uses quantum state coherence to probe transition frequencies in atoms and molecules.

In the ubiquitous two-level Ramsey interferometry experiment [49], an initial population in state $|1\rangle$ is excited into a superposition state $(|1\rangle + |2\rangle)/\sqrt{2}$ by a $\pi/2$ pulse. In the next stage, the superposition state freely evolves and accumulates a relative phase between the states that depends on the driving field detuning from the resonant transition δ. After a free evolution duration τ the population is in the superposition state: $[|1\rangle + |2\rangle \exp(-i\delta\tau)]/\sqrt{2}$. A second identical $\pi/2$ pulse maps the accumulated phase into a time invariant state population that can be read out. For example, the normalized population in $|2\rangle$ will oscillate according to $[1+\cos(\delta\tau)]/2$.

In Ramsey's original experiment, the $\pi/2$ pulses are implemented as two spatially separated interaction regions that an atomic beam passes through. Since the spin precession time τ is fixed by the beam velocity and the distance between the interaction regions, the transition frequency is determined by scanning the driving field's detuning. This approach has been proposed to measure vibrational transition frequencies of NUHFI in a molecular beam experiment using a cavity-enhanced, narrow line width quantum cascade laser [31,50]. In this case, each enantiomer is probed separately to search for PV. Importantly, this interferometer can be used to measure numerous other neutral chiral molecule species since the main requirement is that the molecules are entrainable in a molecular beam as has been demonstrated for a few species [31]. The large molecule count rate compensates for the relatively short interrogation time τ, which is usually limited to a few milliseconds for this type of experiment.

Alternatively, in an experiment where the atoms or molecules are trapped, the Ramsey interrogation sequence can be performed in the time domain. In this case, each $\pi/2$ pulse is applied by modulating the intensity of the driving field. The free evolution time is controlled by the delay between the two $\pi/2$ pulses. The detuning δ is extracted by recording the Ramsey measurements for multiple different free evolution durations (τ) and extracting δ from a fit. These two approaches are nearly equivalent except that the latter enables much longer free evolution durations.

B. Enantiomer-specific state transfer by 3WM

Enantiomer-specific state transfer is a method that uses controlled driving fields to separate enantiomers into different states using quantum interference [40–42,44–47].

In ESST, three states $|1\rangle, |2\rangle, |3\rangle$ are cyclically coupled by fields labeled P, Q, and S that correspond to the transitions $|1\rangle \leftrightarrow |2\rangle$, $|1\rangle \leftrightarrow |3\rangle$, and $|2\rangle \leftrightarrow |3\rangle$, respectively. The applied time-dependent interactions are

$$-\langle \vec{\mu} \cdot \vec{E}_X(t) \rangle = 2\hbar\Omega_X(t)\cos(\omega_X t + \phi_X), \qquad (1)$$

where $X \in \{\mathrm{P}, \mathrm{Q}, \mathrm{S}\}$ and Ω_X, ω_X, and ϕ_X denote the instantaneous Rabi frequency, the driving field frequency and its phase, respectively.

Applying the three fields with three mutually orthogonal polarizations exploits the enantiomer-dependent sign of the scalar triple products of the transition dipole moment components,

$$\vec{\mu}_x^{\mathcal{R}} \cdot (\vec{\mu}_y^{\mathcal{R}} \times \vec{\mu}_z^{\mathcal{R}}) = -\vec{\mu}_x^{\mathcal{S}} \cdot (\vec{\mu}_y^{\mathcal{S}} \times \vec{\mu}_z^{\mathcal{S}}), \qquad (2)$$

to perform enantiomer-dependent processes [38,44]. When these three waves are applied to a racemic sample of chiral molecules, the enantiomer populations are transferred into different quantum states, which allows the detection of the sample's enantiomeric excess, for example. Perfect separation of enantiomers is only achieved if the three fields have a phase relation of

$$\Delta\phi = \phi_{\mathrm{P}} - \phi_{\mathrm{Q}} + \phi_{\mathrm{S}} = \pm\pi/2, \qquad (3)$$

which is required to break the symmetry between states $|2\rangle$ and $|3\rangle$.

This scheme, which has been demonstrated in multiple works using three microwave fields, can theoretically reach perfect transfer of enantiomers into separate states [40–42,44–47]. When the fields are resonant with the transition frequencies, the Hamiltonian describing the interaction under the rotating wave approximation (RWA) is

$$\frac{H_{\mathrm{RWA}}^{\mathrm{3WM}}}{\hbar} = \begin{pmatrix} 0 & \Omega_{\mathrm{P}}(t) & \Omega_{\mathrm{Q}}(t) \\ & 0 & \tilde{\kappa} e^{i\pi/2}\Omega_{\mathrm{S}}(t) \\ \text{c.c.} & & 0 \end{pmatrix}. \qquad (4)$$

To model the sign change of the transition dipole moment, the sign function $\tilde{\kappa}$ is applied without loss of generality to the S transition $\tilde{\kappa}\langle 2|\vec{\mu} \cdot \vec{E}|3\rangle$ [44], where $\tilde{\kappa}(\mathcal{S}) = -1$ and $\tilde{\kappa}(\mathcal{R}) = +1$. For the purpose of this description $\Delta\phi$ is chosen to be $+\pi/2$. The scheme is usually applied at the limit where the maxima of all the instantaneous Rabi frequencies are much larger than any residual detuning on the diagonal elements of $H_{\mathrm{RWA}}^{\mathrm{3WM}}$ such that these may be neglected and the resonance approximation is valid.

ESST is realizable by many approaches using either simultaneous or composite sequences of pulses of the driving fields to change the Rabi frequency in time. In Fig. 2 we consider a racemic sample that is initially in the $|1\rangle$ state. A simultaneous pulse of the P, Q, and S fields results in a full population transfer of the $\mathcal{S}$ enantiomer into $|2\rangle$ and $\mathcal{R}$ into $|3\rangle$.

Since the previous example fully transfers the population of the $\mathcal{S}$ ($\mathcal{R}$) enantiomer from state $|1\rangle$ to the excited state $|2\rangle$ ($|3\rangle$), it is analogous to a π pulse applied to the two-level

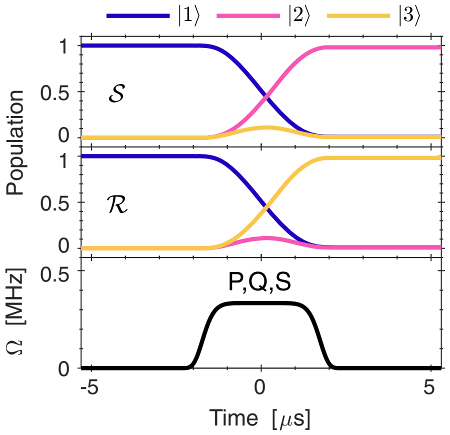

FIG. 2. Enantiomer-specific state transfer using simultaneously applied driving fields as shown in Ref. [44]. Amplitudes of the three relevant states in $\mathcal{S}$ and $\mathcal{R}$ when the P, Q, and S transitions are driven simultaneously at equal maximal Rabi frequencies. While initially both molecules are in $|1\rangle$, after the three pulses the population of $\mathcal{S}$ is transferred to $|2\rangle$ and of $\mathcal{R}$ to $|3\rangle$. If the area of three pulses is halved both enantiomers are in a superposition of all three states.

system. However, if one wishes to adapt ESST into a Ramsey interferometry sequence, the pulses cannot simply be halved in area as is the case for $\pi/2$ pulses in the two-level version of Ramsey spectroscopy (Sec. II A). After the first "half-pulse" both enantiomers occupy a superposition state of all three levels, as can be seen by the midpulse components of $|1\rangle$, $|2\rangle$, and $|3\rangle$ in Fig. 2. Therefore, the state of each enantiomer evolves with multiple frequency components, precluding a straightforward interpretation of any measured oscillating population, reducing enantiomer discrimination and lowering the exhibited fringe contrast. This will culminate in reduced precision and increased susceptibility to systematic shifts for the measurement. In Sec. III we show how to avoid these issues with a different pulse sequence.

C. Switch states for precision measurement

The search for tiny physical effects such as PV is hindered by ambient background effects and instrument fluctuations. Experimentally, these are often suppressed with a differential measurement. This is done by switching the state of the experiment by reversing the relevant parameters and taking the difference of the results. Multiple switches are often used in precision measurements in order to incorporate a differential measurement over more than one dimension [5,51–53].

In this work, we define two user controlled switches. The first describes the quantum level that is read out, which is denoted by the variable $\tilde{\Sigma}$ where the two switch states are $\Sigma^+ = \{\tilde{\Sigma} = +1\}$, which refers to level $|3\rangle$ and $\Sigma^- = \{\tilde{\Sigma} = -1\}$, which refers to level $|2\rangle$. The shorthand symbols Σ^+ and Σ^- enable the reader to know which switch is referenced and the state of that switch. Similarly, the second switch is of the sign of the phase relation $\Delta\phi$ from Eq. (3) and is denoted by the variable $\tilde{\Phi}$, where $\Phi^+ = \{\tilde{\Phi} = +1\}$ refers to the driving field state being $\Delta\phi = +\pi/2$ and $\Phi^- = \{\tilde{\Phi} = -1\}$ refers to $\Delta\phi = -\pi/2$. All the sign functions discussed so far are summarized in Table I.

TABLE I. Switch-state sign function dictionary.

	Phase	State	Chirality
	$\tilde{\Phi}$	$\tilde{\Sigma}$	$\tilde{\kappa}$
+1	$+\pi/2$	$\|3\rangle$	$\mathcal{R}$
−1	$-\pi/2$	$\|2\rangle$	$\mathcal{S}$

Together, $\tilde{\Sigma}$ and $\tilde{\Phi}$ have four measurement configurations or switch states: $(\Sigma^+\Phi^+, \Sigma^-\Phi^+, \Sigma^+\Phi^-, \Sigma^-\Phi^-)$. A certain detuning measured in one of these switch states is denoted as $\delta_{\Sigma^+\Phi^-}$, for example. Any property measured in the experiment in a certain switch state, such as the observed molecule number, carries this labeling.

However, these frequencies do not have an intuitive standalone meaning. Once we have combined them into linear combinations, which are referred to as frequency channels, the various components in the Hamiltonian become distinguishable and the channels become meaningful. One of these frequency channels will isolate the effect in question such as the PV frequency shift, but other channels are also useful for monitoring and analyzing sources of systematic uncertainty.

A frequency channel is labeled $f_{\Phi\Sigma}$ when the linear combination is *odd* with respect to both the $\tilde{\Phi}$ and $\tilde{\Sigma}$ switches, while a channel is labeled f_Σ when the linear combination is *odd* with respect to the $\tilde{\Sigma}$ switch and *even* with respect to the $\tilde{\Phi}$ switch. If the investigated effect is not the dominant term in any frequency channel, then more switches need to be added, as we show in the Appendix. All switch states must be measured to compute the values for frequency channels in what is known as a data block. For each channel the mean value, standard error, and other statistical quantities are extracted from multiple blocks.

The concept of linear combinations that form channels can be applied to other properties that are measured and not only to frequencies. These include fringe contrast, phase offsets, laser powers, quantum state populations, and many others. See Ref. [54], for example, where five experimental switches are employed. These 32 states are combined into channels for five different types of properties including transition frequency. In this work we describe only the frequency channels since one of them corresponds to the PV shift.

III. EMBEDDING RAMSEY SPECTROSCOPY WITHIN 3WM

For our scheme, we developed a pulse sequence to perform two simultaneous Ramsey spectroscopies in a three-level system (Fig. 1). Each enantiomer is excited to a unique superposition using the sign difference between the scalar triple products of their transition dipole moment components [Eq. (2)]. Analogously to two-state Ramsey spectroscopy (Sec. II A), a second excitation allows us to measure the energy difference of each superposition in separate final states. We apply the method to vibrational transitions where PV is enhanced throughout the rest of this work. However, the method could be applied to ongoing experiments with microwave rotational transitions for precision spectroscopy of PV [30,46].

A. Hamiltonian

As in ESST (Sec. II B), three states are coupled by fields along the P, Q, and S transitions [Eq. (1)] with mutually orthogonal polarizations to interact with all three electric dipole components. The phase constraints of $\Delta\phi = \pm\pi/2$ of Eq. (3) are also maintained for the fields as in ESST. However, here we allow the fields driving the transitions P, Q, and S to be detuned from resonance by a frequency δ_P, δ_Q, and δ_S, respectively, in contrast to Sec. II B.

The off-resonance energy level diagram for the $\mathcal{S}$ and $\mathcal{R}$ enantiomers is depicted in Fig. 1(b). To simplify the interaction from the general off-resonance description, we choose the driving field frequencies such that $\omega_\mathrm{Q} - \omega_\mathrm{P} = \omega_\mathrm{S}$, which means that for the detunings,

$$\delta_\mathrm{Q} - \delta_\mathrm{P} = \delta_\mathrm{S}, \tag{5}$$

Applying the RWA, the Hamiltonian describing the interaction for the two $\tilde{\Phi}$ switch states and both enantiomers $\tilde{\kappa}$ is

$$\frac{H^{\tilde{\Phi}\tilde{\kappa}}_\mathrm{RWA}}{\hbar} = \begin{pmatrix} 0 & \Omega_\mathrm{P}(t) & \Omega_\mathrm{Q}(t) \\ & \delta - \delta_\mathrm{S}/2 + \tilde{\kappa}\Delta^\mathrm{vib}_\mathrm{PV} & \tilde{\Phi}\,\tilde{\kappa}\, e^{i\pi/2}\Omega_\mathrm{S}(t) \\ \mathrm{c.c.} & & \delta + \delta_\mathrm{S}/2 + \tilde{\kappa}\Delta^\mathrm{vib}_\mathrm{PV} \end{pmatrix}. \tag{6}$$

Here we have substituted $\delta = (\delta_\mathrm{P} + \delta_\mathrm{Q})/2$, the mean detuning from the vibrational transitions. Therefore, using Eq. (5) the detunings from $|1\rangle$ to states $|2\rangle$ and $|3\rangle$ are simply $\delta \mp \delta_\mathrm{S}/2 = \delta + \tilde{\Sigma}\delta_\mathrm{S}/2$, respectively. These are the diagonal elements (2, 2) and (3, 3) of $H^{\tilde{\Phi}\tilde{\kappa}}_\mathrm{RWA}$ before including PV. This substitution strategy to a common mean value and antisymmetric component for the detunings will be convenient later in Sec. III C.

To include the PV energy shift of each enantiomer we add $\tilde{\kappa}\Delta^\mathrm{vib}_\mathrm{PV}$, where $\tilde{\kappa}$ is the sign function representing the handedness of the molecule [$\tilde{\kappa}(\mathcal{S}) = -1$, $\tilde{\kappa}(\mathcal{R}) = +1$]. The choice to label $\Delta^\mathrm{vib}_\mathrm{PV}$ as the antisymmetric shift of the vibrational transition due to PV is made for convenience and leads to a total relative shift of $2\Delta^\mathrm{vib}_\mathrm{PV}$ as depicted in Fig. 1(b). Note that in contrast to $H^\mathrm{3WM}_\mathrm{RWA}$ [Eq. (4)], where enantiomer separation is the goal, the detunings of the driving fields δ and δ_S cannot be neglected here, since we expect $\Delta^\mathrm{vib}_\mathrm{PV}$, our subject of interest, to be small relative to these.

The intensity of the three driving fields can be individually controlled in a time-dependent manner such that the instantaneous Rabi frequencies Ω_P, Ω_Q, and Ω_S are also time dependent [Fig. 1(c)]. To model the sign change of the transition dipole moment, $\tilde{\kappa}$ is applied to the S transition $\tilde{\kappa}\langle 2|\vec{\mu}\cdot\vec{E}|3\rangle$ [44] as discussed in Sec. II B. The sign of the relative phase from Eq. (3), $\tilde{\Phi} = \pm 1$, is also applied to the S transition term without loss of generality using the relation $e^{\pm i\pi/2} = \tilde{\Phi}e^{i\pi/2}$ (Sec. II C). This notation highlights the interchangeability of $\tilde{\Phi}$ and $\tilde{\kappa}$ except that the former is a user controlled switch, while the latter is a property of the investigated molecule.

The goal of the rest of this work is to utilize the user controlled switches $\tilde{\Phi}$ and $\tilde{\Sigma}$ in a series of measurements to separate $\Delta^\mathrm{vib}_\mathrm{PV}$ from the rest of the terms in $H^{\tilde{\Phi}\tilde{\kappa}}_\mathrm{RWA}$ using the fact that $\tilde{\kappa}$ appears in an off-diagonal interaction element and multiplies $\Delta^\mathrm{vib}_\mathrm{PV}$. These measurements are performed by driving the P, Q, and S interaction fields, which control the off-diagonal Rabi frequencies, in a specific pulse sequence. $\tilde{\Sigma}$ is a controlled switch in the sense that we label which state to read out, but these two states may also be read out simultaneously.

B. Pulsed sequence outline

Our scheme begins with both $\mathcal{S}$ and $\mathcal{R}$ enantiomers populating state $|1\rangle$. Following Fig. 3(a) for the $\tilde{\Phi} = -1$ ($\Delta\phi = -\pi/2$) case, the first "$\pi/2$" pulse sequence creates the enantiomer-specific superposition states:

$$|\mathcal{S}\rangle = (|1\rangle - i|2\rangle)/\sqrt{2},$$
$$|\mathcal{R}\rangle = (|1\rangle - i|3\rangle)/\sqrt{2}. \tag{7}$$

This sequence is composed of two pulses: a simultaneous application of the fields along the P and Q transitions (PQ1) followed by driving the S transition (S1). Next the molecules freely evolve according to the Hamiltonian, $H^{\tilde{\Phi}\tilde{\kappa}}_\mathrm{free}$, which is equal to $H^{\tilde{\Phi}\tilde{\kappa}}_\mathrm{RWA}$ [Eq. (6)] with $\Omega_\mathrm{P} = \Omega_\mathrm{Q} = \Omega_\mathrm{S} = 0$. After evolving for a duration τ, we apply the second $\pi/2$ pulse sequence to stop the phase evolution. This second sequence consists of a second S pulse (S2), followed by P and Q pulses applied together again (PQ2), and finally another S pulse (S3) (see Sec. III D for pulse areas and intermediate quantum states).

The resulting population in states $|2\rangle$ and $|3\rangle$ is related to the projections onto these states. We refer to the final states $|2\rangle$ and $|3\rangle$ by the shorthand $|\tilde{\Sigma}\rangle$ and to $|\mathcal{S}\rangle$ and $|\mathcal{R}\rangle$, the two states after the first $\pi/2$ pulse sequence from Eq. (7), as $|\tilde{\kappa}\rangle$. The normalized populations as a function of τ are depicted in Fig. 3(b) and are given by

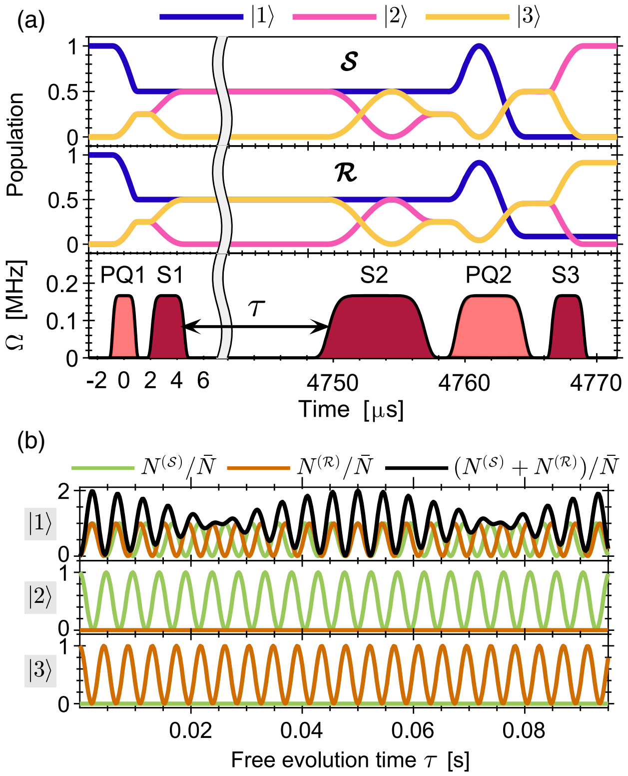

FIG. 3. Simulation of the pulse sequence with multiple delays τ for simultaneous Ramsey spectroscopy of both enantiomers showing enantiomer-specific oscillations in states $|2\rangle$ and $|3\rangle$. The difference between these detunings can be used to extract $\Delta_{\mathrm{PV}}^{\mathrm{vib}}$. The pulse sequence for a free evolution time of 4.7 ms (single fringe) is shown in (a) along with the time-dependent magnitudes of the wave functions of states $|1\rangle$, $|2\rangle$, and $|3\rangle$ for $\mathcal{S}$ and $\mathcal{R}$ enantiomers. Here $\tilde{\Phi} = -1$, $\delta_{\mathrm{S}} = 0$, and $\delta = 2\pi \times 220$ Hz. Simultaneous pulses along the P and Q transitions with identical temporal shapes are denoted by the PQ symbol. The pulse areas of PQ1, S1, S2, PQ2, and S3 are $\pi/\sqrt{32}$, $\pi/4$, $3\pi/4$, $3\pi/\sqrt{32}$, and $\pi/4$, respectively (see Sec. III D). While $\mathcal{S}$ enantiomers undergo exactly one cycle, $\mathcal{R}$ enantiomers are slightly past the top of the fringe due to the $\Delta_{\mathrm{PV}}^{\mathrm{vib}} = 2\pi \times 10$ Hz difference. The resulting normalized populations for each enantiomer, $N^{(\mathcal{S})}/\bar{\mathrm{N}}$ and $N^{(\mathcal{R})}/\bar{\mathrm{N}}$, in states $|1\rangle$, $|2\rangle$, and $|3\rangle$ of the Ramsey sequence are plotted in (b) as a function of free evolution time τ.

$$\begin{aligned}\frac{N_{\tilde{\Phi},\tilde{\Sigma}}(\tau)}{\bar{N}} &= \frac{1}{2}\left[\cos(\delta_{\tilde{\Phi},\tilde{\Sigma}}\tau)) + 1\right] \\ &= \left\|\langle\tilde{\Sigma}|U_{2^{\mathrm{nd}}}^{\pi/2}\exp\left(-iH_{\mathrm{free}}^{\tilde{\Phi}\,\tilde{\kappa}}\tau/\hbar\right)|\tilde{\kappa}\rangle\right\|^{2}, \end{aligned} \tag{8}$$

$$\begin{aligned}\delta_{\tilde{\Phi},\tilde{\Sigma}} &= \delta + \tilde{\Sigma}\frac{\delta_{\mathrm{S}}}{2} + \tilde{\kappa}\Delta_{\mathrm{PV}}^{\mathrm{vib}} \\ &= \delta + \tilde{\Sigma}\frac{\delta_{\mathrm{S}}}{2} - \tilde{\Phi}\,\tilde{\Sigma}\,\Delta_{\mathrm{PV}}^{\mathrm{vib}}, \end{aligned} \tag{9}$$

where $\bar{N}$ is the mean number of molecules of each enantiomer that is detected in a repetition of the experiment and $U_{2^{\mathrm{nd}}}^{\pi/2}$ denotes the second $\pi/2$ pulse sequence. Note that the detunings in Eq. (9) are simply the diagonal elements of $H_{\mathrm{RWA}}^{\tilde{\Phi}\,\tilde{\kappa}}$ [Eq. (6)]. Using the relation $\tilde{\kappa} = -\tilde{\Phi}\cdot\tilde{\Sigma}$ we convert these detunings into experimentally set switch states $\tilde{\Phi}$ and $\tilde{\Sigma}$ as opposed to $\tilde{\kappa}$ which is implicitly known in the simulation. This relation can be understood by considering the switch state $\tilde{\Phi} = -1$ plotted in Fig. 3(b), where we expect to find $\mathcal{S}$ enantiomers ($\tilde{\kappa} = -1$) in state $|2\rangle$ ($\tilde{\Sigma} = -1$). Switching either $\tilde{\Phi}$ or measuring $|3\rangle$ ($\tilde{\Sigma} = +1$) in turn changes the enantiomer.

We apply a realistic $\Delta_{\mathrm{PV}}^{\mathrm{vib}} = 2\pi \times 10$ Hz as calculated for NUHFI [25], for example, which causes the slightly different frequencies for the populations of $\mathcal{S}$ and $\mathcal{R}$ in Fig. 3(b), where we have taken $\delta_{\mathrm{S}} = 0$ to highlight $\Delta_{\mathrm{PV}}^{\mathrm{vib}}$ in the plot. While these two oscillations are fully resolved in states $|2\rangle$ and $|3\rangle$ for each enantiomer, they mix in $|1\rangle$ where the $\mathcal{S}$ and $\mathcal{R}$ populations beat.

The populations in states $|2\rangle$ and $|3\rangle$ need to be measured for various values of τ in order to extract the detuning of each enantiomer's superposition as described in Sec. II A. Population detection can be achieved by single-photon photodissociation of the molecule and separating the photofragments according to their kinetic energies [20], via velocity map imaging [55], for example [Fig. 1(d)]. If needed, the kinetic energy difference can be amplified by further excitation of the population in one of these states.

Note that there may exist other pulse sequences that achieve our goal. For simplicity, we ignore the possible rotational degeneracy in states $|1\rangle$, $|2\rangle$, and $|3\rangle$, which would reduce fringe contrast. To remedy such a situation, the initial state $|1\rangle$ can be assumed to have a rotational quantum number of $J = 0$. Alternatively, it is possible to lift the degeneracy using an external field, or use more complicated 3WM pulse sequences as well as circular polarization to avoid such issues as proposed for ESST [47]. In principle, such sequences may solve this issue for the 3WM version of Ramsey spectroscopy.

C. Isolating PV using switch states

Since the difference between the oscillation frequencies of the populations of $|3\rangle$ and $|2\rangle$ is

$$\delta_{\tilde{\Phi},\Sigma^{+}} - \delta_{\tilde{\Phi},\Sigma^{-}} = \delta_{\mathrm{S}} - 2\tilde{\Phi}\Delta_{\mathrm{PV}}^{\mathrm{vib}},$$

according to Eq. (9), an additional switch of the experimental configuration $\tilde{\Phi}$ must be used to isolate $\Delta_{\mathrm{PV}}^{\mathrm{vib}}$. When the relative phase of the fields is switched to $\tilde{\Phi} = +1$ ($\Delta\phi = \pi/2$), the roles of states $|2\rangle$ and $|3\rangle$ are reversed. In this case, the superposition states formed in the Ramsey sequence are $|\mathcal{S}\rangle = (|1\rangle - i|3\rangle)/\sqrt{2}$ and $|\mathcal{R}\rangle = (|1\rangle - i|2\rangle)/\sqrt{2}$.

The detunings of all four switch states or configurations $\{\tilde{\Phi},\tilde{\Sigma}\} = \{\pm1,\pm1\}$ must be measured to complete a data

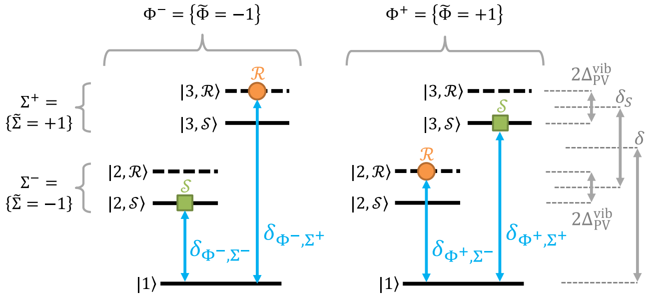

FIG. 4. The rotating frame level diagram is shown including the weak force PV component. The detunings of the four switch-state transitions acquired during the experiment sequence are depicted by the blue arrows [Eq. (9)]. Each arrow corresponds to a different experimental configuration of the "phase" and the detected "state" denoted by $\tilde{\Phi}$ and $\tilde{\Sigma}$, respectively (Table I). All four linear combinations of these switches form frequency channels [Eq. (10)], where $4\Delta_{\mathrm{PV}}^{\mathrm{vib}} = (\delta_{\Phi^-,\Sigma^+} - \delta_{\Phi^-,\Sigma^-}) - (\delta_{\Phi^+,\Sigma^+} - \delta_{\Phi^+,\Sigma^-})$. Since it is possible in principle to measure δ_{Φ^-,Σ^+} and δ_{Φ^-,Σ^-} in the same shot as well as δ_{Φ^+,Σ^+} and δ_{Φ^+,Σ^-}, the scheme can benefit from common-mode noise rejection on the PV frequency channel.

block. These detunings are plotted on the rotating frame level diagram in Fig. 4. The linear combinations of these switch states form frequency channels, which have intuitive physical meaning, as shown below:

$$2\pi\begin{pmatrix} f_0 \\ f_\Phi \\ f_\Sigma \\ f_{\Phi\Sigma} \end{pmatrix} \equiv \frac{1}{4}\begin{pmatrix} + & + & + & + \\ + & + & - & - \\ + & - & + & - \\ + & - & - & + \end{pmatrix}\begin{pmatrix} \delta_{\Phi^+,\Sigma^+} \\ \delta_{\Phi^+,\Sigma^-} \\ \delta_{\Phi^-,\Sigma^+} \\ \delta_{\Phi^-,\Sigma^-} \end{pmatrix} = \begin{pmatrix} \delta \\ 0 \\ \delta_S/2 \\ -\Delta_{\mathrm{PV}}^{\mathrm{vib}} \end{pmatrix}. \tag{10}$$

To us, $f_{\Phi\Sigma}$ is the most important frequency channel since it is both Φ odd and Σ odd, thus isolating the PV component of the two vibrational transitions of $\mathcal{S}$ and $\mathcal{R}$. The other channels are used to tune the experiment and to probe sources of systematic error. For example, the f_Σ channel can be used to measure any Σ-odd effects between states $|2\rangle$ and $|3\rangle$ such as Zeeman shifts with different g factors for the states (see the Appendix). These can be corrected with a δ_S offset.

When states $|2\rangle$ and $|3\rangle$ are measured simultaneously in a resolved manner, the two Σ-odd channels, f_Σ and $f_{\Phi\Sigma}$, benefit from common-mode noise suppression. This includes dissociation laser noise, which can be classified as proportional number noise, and magnetic field noise, which manifests as frequency noise. Number noise effects cancel to first order when taking the difference of $N_{\tilde{\Phi},\Sigma^+} - N_{\tilde{\Phi},\Sigma^-}$. Importantly, frequency noise effects are also suppressed for such a term when $N_{\tilde{\Phi},\Sigma^+}$ and $N_{\tilde{\Phi},\Sigma^-}$ are in phase. Similar noise rejection has been demonstrated to achieve the SQL in a noisy photodissociation measurement of the permanent electric dipole moment of the electron (eEDM) [48,53].

According to the SQL when perfect contrast is assumed, the uncertainty on $f_{\Phi\Sigma}(\propto \Delta_{\mathrm{PV}}^{\mathrm{vib}})$ scales as $(T\sqrt{N})^{-1}$, where T is the coherence time and N is the number of molecules detected. When considering a beam experiment [31] or a trapped molecule experiment (as we plan with trapped molecular ions), reasonable coherence times to expect are $T = 1$ ms or $T = 100$ ms, respectively. This means that detection of only 10^8 or 10^4 molecules, respectively, would be needed to reach an uncertainty of 0.1 Hz as opposed to a much higher number depending on the technical noise if the SQL cannot be reached. This precision is far below the limit required to measure $\Delta_{\mathrm{PV}}^{\mathrm{vib}}$ for NUHFI, for example, which potentially could be interrogated in a beam experiment, assuming the species could be synthesized in sufficient quantity.

This precision is also sufficient to observe PV in an experiment using trapped CHDBrI^+ [19,20]. In this case the prochiral counterpart $\mathrm{CH_2BrI}$ is commercially available in bottled form such that obtaining a bottle of the neutral precursor CHDBrI is also feasible. The required 10^4 molecules of CHDBrI^+ measured as computed above is minuscule when considering 10^8 HfF^+ molecules measured in the latest eEDM experiment, where the molecule is formed through a reaction with a laser ablated metal [53].

Drifts of the ambient conditions will be suppressed regardless of their rate in the proposed simultaneous measurement, as opposed to any implementation where the probed enantiomer is switched, which would limit the bandwidth of the noise rejected, such as in Ref. [30] where switching enantiomers takes several minutes.

Alternatively, if simultaneous measurement is not possible, the two states can also be read out sequentially by any state-selective technique such as fluorescence, state-selective photoionization or photodissociation, or state-dependent chemistry. This slightly reduces the number of suppressed noise sources, but significant noise reduction is maintained in spite of the sequential readout since the Ramsey free evolution occurs simultaneously. Moreover, the simultaneous free evolution relaxes the required relative stability to measure $\Delta_{\mathrm{PV}}^{\mathrm{vib}}$ to 10^{-9} for NUHFI as opposed to 10^{-13} when comparing independently probed vibrational transitions. This is because $\Delta_{\mathrm{PV}}^{\mathrm{vib}}$ is compared to $|\omega_{\mathrm{P}} - \omega_{\mathrm{S}}|$, the rotational splitting, and not the vibrational transition.

D. Pulse sequence description

To explain the pulse sequences used to create the composite $\pi/2$ pulses, we describe a specific case of the Hamiltonian [Eq. (6)], where $\phi_{\mathrm{P}} = \phi_{\mathrm{Q}}$ such that $\Delta\phi = \phi_{\mathrm{S}} = -\pi/2$ $(\tilde{\Phi} = -1)$ and $\delta_{\mathrm{S}} = 0$. This simplification isolates the S pulses as those that discriminate between $\mathcal{S}$ and $\mathcal{R}$ molecules for a clearer description. Following Fig. 3(a), the first $\pi/2$ pulse sequence begins with a simultaneous application of the fields driving the P and Q transitions (denoted PQ1), each with an area of $\pi/\sqrt{32}$ to create the superposition

$$|\mathcal{S}\rangle = |\mathcal{R}\rangle = \frac{1}{\sqrt{2}}|1\rangle - \frac{i}{2}(|2\rangle + |3\rangle).$$

To complete the first $\pi/2$ sequence an S pulse with an area of $\pi/4$ is applied (denoted S1), separating the enantiomers in $|2\rangle, |3\rangle$ to the unique superposition states $|\mathcal{S}\rangle = (|1\rangle - i|2\rangle)/\sqrt{2}$ and $|\mathcal{R}\rangle = (|1\rangle - i|3\rangle)/\sqrt{2}$. Both states evolve freely for a time τ to

$$|\mathcal{S}\rangle = (|1\rangle - i|2\rangle e^{-i\delta^{\mathcal{S}}\tau})/\sqrt{2},$$
$$|\mathcal{R}\rangle = (|1\rangle - i|3\rangle e^{-i\delta^{\mathcal{R}}\tau})/\sqrt{2}$$

before the second $\pi/2$ pulse sequence is applied to translate the phase evolution of each enantiomer to oscillating populations in $|2\rangle, |3\rangle$ separately. The second $\pi/2$ pulse sequence begins with an S pulse of area $3\pi/4$ (denoted S2) that reverses the effect of S1, by completing its area to π and leading to the state

$$|\mathcal{S}(\mathcal{R})\rangle = \frac{1}{\sqrt{2}}|1\rangle + \frac{i}{2}(|2\rangle + |3\rangle)e^{-i\tau\delta^{\mathcal{S}(\mathcal{R})}}.$$

Here the two wave functions are written in a shortened notation for $\mathcal{S}$ with the corresponding $\mathcal{R}$ wave function in parentheses, where $\delta^{\mathcal{S}} = \delta_{\Phi^-,\Sigma^-}$ and $\delta^{\mathcal{R}} = \delta_{\Phi^-,\Sigma^+}$ correspond to the detuning for each enantiomer [Eq. (9)]. The S2 pulse symmetrizes the overall state relative to $|2\rangle$ and $|3\rangle$ before the second simultaneous PQ pulse (denoted PQ2) is applied. The PQ2 pulse has an area of $3\pi/\sqrt{32}$ and once applied the resulting state becomes

$$|\mathcal{S}(\mathcal{R})\rangle = \sin\left(\tau\delta^{\mathcal{S}(\mathcal{R})}/2\right)|1\rangle + \frac{\cos(\tau\delta^{\mathcal{S}(\mathcal{R})}/2)}{\sqrt{2}}(|2\rangle + |3\rangle).$$

Alternatively, an identical pulse to PQ1 could be applied, but the resulting oscillations would be shifted by a π phase offset. Finally, the sequence is completed with an S pulse (denoted S3) that is identical to S1 which transcribes the progression of the phase evolution to states $|2\rangle$ and $|3\rangle$ for $\mathcal{S}$ and $\mathcal{R}$ enantiomers, respectively. The resulting states and populations are

$$|\mathcal{S}\rangle = \sin(\tau\delta^{\mathcal{S}}/2)|1\rangle + \cos(\tau\delta^{\mathcal{S}}/2)|2\rangle,$$
$$|\mathcal{R}\rangle = \sin(\tau\delta^{\mathcal{R}}/2)|1\rangle + \cos(\tau\delta^{\mathcal{R}}/2)|3\rangle$$
$$\Rightarrow \|\langle 2|\mathcal{S}\rangle\|^2 = \frac{1+\cos(\tau\delta^{\mathcal{S}})}{2} = \frac{1+\cos(\tau(\delta - \Delta_{\mathrm{PV}}^{\mathrm{vib}}))}{2}$$
$$\Rightarrow \|\langle 3|\mathcal{R}\rangle\|^2 = \frac{1+\cos(\tau\delta^{\mathcal{R}})}{2} = \frac{1+\cos(\tau(\delta + \Delta_{\mathrm{PV}}^{\mathrm{vib}}))}{2}.$$

Here we have substituted the individual enantiomer's detuning from its respective state, $\delta^{\mathcal{S}}$ and $\delta^{\mathcal{R}}$, by the specific detuning of the switch state with $\delta_{\mathrm{S}} = 0$ according to Eqs. (8) and (9). Figure 3(a) shows a single fringe cycle for $\mathcal{S}$ molecules ($\tau = 2\pi/\delta^{\mathcal{S}}$) with the resulting populations

$$\|\langle 2|\mathcal{S}\rangle\|^2 = 1,$$
$$\|\langle 3|\mathcal{R}\rangle\|^2 = \left[1 + \cos\left(2\pi\frac{2\Delta_{\mathrm{PV}}^{\mathrm{vib}}}{\delta^{\mathcal{S}}}\right)\right]/2$$
$$\approx 1 - \left(\frac{2\pi\Delta_{\mathrm{PV}}^{\mathrm{vib}}}{\delta^{\mathcal{S}}}\right)^2.$$

This case shows how the PV signature can be isolated, but the population of $\mathcal{R}$ molecules in state $|3\rangle$ scales quadratically with the small shift $\Delta_{\mathrm{PV}}^{\mathrm{vib}}$ due to the selected τ near the top of the fringe. Naturally, for a precision measurement the side of the fringe would be preferred such that $\tau = (2\pi n + \frac{\pi}{2})/\delta$ should be chosen, for an integer n where the scaling is linear. The resulting populations are

$$\|\langle 2|\mathcal{S}\rangle\|^2\left(\|\langle 3|\mathcal{R}\rangle\|^2\right) = \left[1 - \sin\left(\left(2\pi n + \frac{\pi}{2}\right)\frac{\tilde{\kappa}\Delta_{\mathrm{PV}}^{\mathrm{vib}}}{\delta}\right)\right]\Big/2$$
$$\approx \frac{1}{2} - \left(\pi n + \frac{\pi}{4}\right)\frac{\tilde{\kappa}\Delta_{\mathrm{PV}}^{\mathrm{vib}}}{\delta},$$

where $\tilde{\kappa}$ describes the handedness of the molecule according to $\mathcal{S}$ and $\mathcal{R}$. To also enjoy the benefits of noise cancellation n should be chosen such that the two enantiomers' fringes are in phase.

While we described the pulse pattern for a specific case, it also works for $\delta_{\mathrm{S}} \neq 0$ and $\phi_{\mathrm{P}} \neq \phi_{\mathrm{Q}}$ with the $\tilde{\Phi}$ switch needed to isolate $\Delta_{\mathrm{PV}}^{\mathrm{vib}}$ as shown in Eq. (10).

E. Scheme sensitivity to experimental parameters

In order to test our sensitivity to changes in the experiment parameters, we varied the relative areas of each of the pulses in the sequence. We define the contrast of the fringe in state $\tilde{\Sigma}$ as

$$C_{\tilde{\Sigma}} = \left|\mathcal{N}_{\tilde{\Sigma}}^{(\mathcal{S})} - \mathcal{N}_{\tilde{\Sigma}}^{(\mathcal{R})}\right|/\bar{N}, \tag{11}$$

where $\mathcal{N}_{\tilde{\Sigma}}^{(\tilde{\kappa})}$ is the amplitude of the population oscillation of the enantiomer $\tilde{\kappa}$ in state $\tilde{\Sigma}$. We also define the leakage for both switch states of $\tilde{\Phi}$ as

$$\mathrm{Leakage}_{\Phi^\pm} = \left(\mathcal{N}_{\Sigma^\mp}^{(\mathcal{S})} + \mathcal{N}_{\Sigma^\pm}^{(\mathcal{R})}\right)/2\bar{N}. \tag{12}$$

This value describes the average amplitude of the contaminant enantiomer that is not expected in each state for perfect pulses (violates the $\tilde{\kappa} = -\tilde{\Phi}\cdot\tilde{\Sigma}$ mapping). For example, in the case of $\tilde{\Phi} = -1$ the leakage from Eq. (12) reads as $(\mathcal{N}_{|3\rangle}^{(\mathcal{S})} + \mathcal{N}_{|2\rangle}^{(\mathcal{R})})/2\bar{N}$.

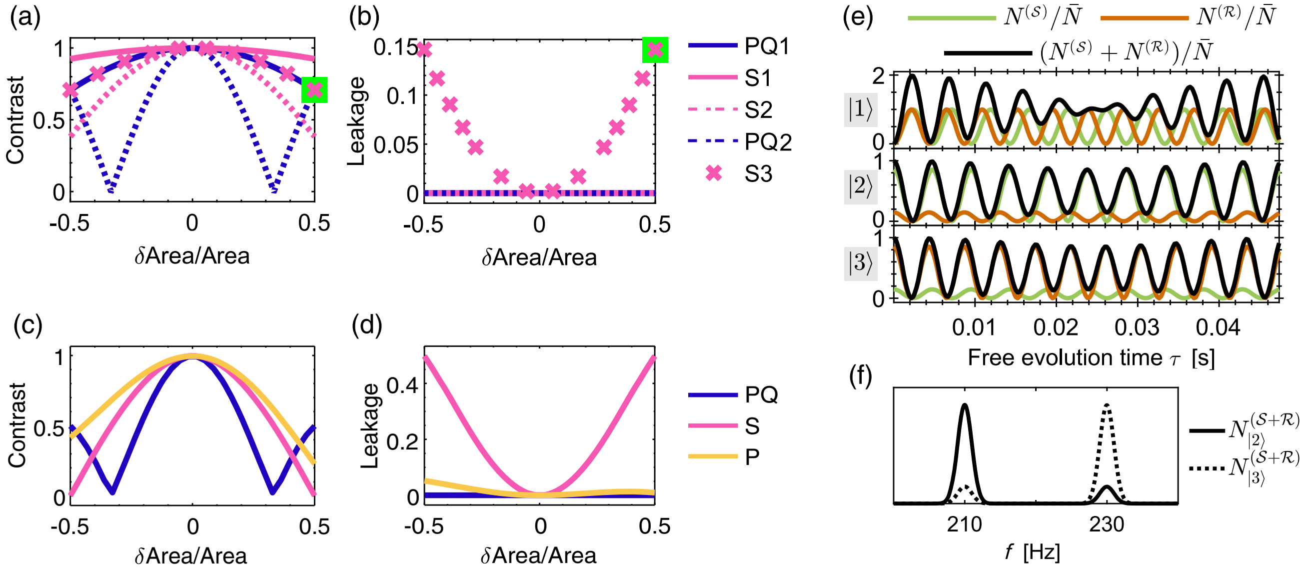

FIG. 5. Experimental requirements for tuning accuracy and stability of the various driving fields of the sequence. We consider the reduction of the contrast [Eq. (11)] and leakage of an unexpected enantiomer [Eq. (12)] due to an inaccurately tuned area of each pulse (a),(b) as well as an instability of the driving field power acting on all pulses for the same transition (c),(d). (e) A Ramsey sequence, showing significant oscillation contamination of the wrong enantiomer (leakage) for $\tilde{\Phi} = -1$, is created with a variation of 50% in S3 [green squares in (a) and (b)]. This contamination can be observed in the spectra of the total populations (f), but would only lead to an underestimation of total shift of $2\Delta_{\mathrm{PV}}^{\mathrm{vib}} = 2 \times 2\pi \times 10$ Hz. Since this is a noiseless simulation the lines are broadened to a 1 Hz standard deviation.

While a low $C_{\tilde{\Sigma}}$ leads to a reduced precision of the measurement, a high leakage can lead to a systematic shift of $f_{\Phi\Sigma} (\propto \Delta_{\mathrm{PV}}^{\mathrm{vib}})$. However, we find that moderate tuning errors of experiment parameters lead to minimal leakage and contrast loss. The contrast and leakage are plotted in Figs. 5(a) and 5(b) for a variation of each pulse area. When these variations are stabilized to within 10%, the contrast is more than 0.88 and the leakage is less than 0.01. We also study the stability requirements of the driving field intensities, by considering a variation of the area of all pulses in the sequence of the same transition. We find that the issue is slightly worse than for the previous case of initial tuning errors as shown in Figs. 5(c) and 5(d). However, the leakage for a 10% change in the area of each S pulse, which is applied three times, remains smaller than 0.04. Importantly, the contrast and leakage vary quadratically around the ideal set point for all of these parameters.

Figure 5(c) shows a case with substantial leakage in the fringes due to a large 50% error in the area of pulse S3. The spectrum observed in states $|2\rangle$ and $|3\rangle$ shows the opposite enantiomer frequency as a small feature on the sides of the main peaks [Fig. 5(d)]. This leakage may seem to be a detrimental systematic in the scheme, but would only lead to an underestimation of $\Delta_{\mathrm{PV}}^{\mathrm{vib}}$ with no phantom PV frequency appearing. A similar argument can be made if the $\tilde{\Sigma}$ state readout is not fully resolved.

F. Advantages toward precision measurement

To further emphasize the advantages of our method, where the Ramsey scheme is embedded within the three-level system, we compare to an alternative straightforward scheme where vibrational Ramsey spectroscopy is performed between two states (a ground and excited vibrational level) of the molecules in a racemic sample followed by a subsequent microwave 3WM enantiomer-selective transfer step using three rotational states of the excited vibrational level. Notably, both the embedded and sequential schemes should have near perfectly enantiomer-resolved frequencies since all the vibrationally excited states are unpopulated, as opposed to the case where the 3WM step precedes Ramsey spectroscopy. While the two schemes have similar experimental complexity, both requiring at least one stable laser and at least one microwave field, our proposed embedded scheme has significant advantages.

The first important advantage to precision measurement stems from the benefits of monitoring possible sources of systematic uncertainty such as ambient magnetic fields. In both schemes, multiple experimental switches must be incorporated into linear combinations of the observed frequencies to isolate $\Delta_{\mathrm{PV}}^{\mathrm{vib}}$ [Eq. (10)]. The other combinations are used to monitor other components of the Hamiltonian. In the Appendix, we show how an additional switch of the sign of δ_S can be used to measure an ambient magnetic field *in situ*, due to the lever arm that arises from the different g factors of the rotational states $|2\rangle$ and $|3\rangle$. This *in situ* magnetometer-type measurement is not possible for the straightforward nonembedded scheme since the same ground and excited states are used for both enantiomers. While auxiliary measurements with external magnetometers are possible to estimate the possible systematics, they are not as precise as those detected by the molecules themselves, which is crucial to precision measurement as discussed by Wu *et al.* [56]. Additional switches can be used to isolate other effects caused by the surroundings.

A second important advantage concerns maintaining the measurement precision on PV at the SQL or quantum projection noise limit toward new physics searches [17], once a nonzero PV is hypothetically observed. Importantly, common-mode noise rejection only works if the two simultaneously measured sine waves are nearly in phase [48]. If PV is large enough to cause a substantial phase shift between the enantiomers, then many noise sources can no longer be considered to be common mode. While for a beam experiment such as Ref. [31] the expected coherence time of ~1 ms would induce a negligibly small phase shift, the shift would be large when considering an experiment using trapped molecular ions, where the expected coherence time is ~100 ms, even for PV shifts significantly smaller than $2\pi \times 10$ Hz. However, in our scheme, purposefully applied δ_S corrections can be used to bring the two sine waves in phase without waiting for a beating of the frequencies. This capability is crucial for searches for time variation in the signal such as in dark matter sensing [17], for example. There, the ability to bring the fringes in phase at arbitrary, long evolution times enables the high frequency range to be measured at the SQL.

G. Experimental feasibility

We now describe the experimental feasibility of our proposed method. The choice of the rotational levels $|2\rangle$, $|3\rangle$ in $v = 1$ and level $|1\rangle$ in $v = 0$ is not only taken to enhance the PV energy difference relative to pure rotational transitions [8,31], it also avoids the thermal population contamination that exists in rotationally excited states, which harms the transfer contrast as pointed out by Leibscher *et al.* [44] among others and directly proven experimentally by Lee *et al.* [46] These types of vibrational transitions are often situated in the midinfrared to long-infrared wavelength range, where laser stabilization is challenging. Fortunately, adequately narrow lasers for coherent excitation in this range have already been demonstrated [31,50]. Alternatively, an optical parametric oscillator laser can be used [45]. Connecting pure rotational transitions such as states $|2\rangle$ and $|3\rangle$ is ubiquitous in microwave 3WM schemes. Additionally, the scheme requires specific timings of pulses for the three transitions. In the microwave regime the timings can be set using microwave sources or amplifiers, but for the IR lasers, acousto-optic modulators, which are available in this wavelength range (or another alternative), are required to implement the pulses.

Since it is technically feasible, our analysis assumes that the fields applied have sufficiently narrow linewidth relative to the target free evolution time τ between the two applied composite $\pi/2$ pulses to avoid fringe decoherence. This is also required to set the phase condition of Eq. (3) to efficiently separate the enantiomers. For trapped molecular ion experiments which may have coherence times on the second scale [48,53], the available linewidths are near the current feasible limit. Interestingly, if the two IR transitions originate from the same laser via modulation at the microwave transition frequency by an electro-optic modulator, the phase condition of Eq. (3) can be achieved for a relatively broad linewidth laser by common-mode phase stability. This way, the separation of enantiomers would be guaranteed while the coherence time of the Ramsey sequence alone would be compromised by the linewidth, thereby reducing the susceptibility to shifts arising from leakage as discussed above.

Multiple other mechanisms can cause decoherence of the molecules between the two applied composite $\pi/2$ pulses which originate from sources such as collisions, inhomogeneous magnetic fields, in addition to noise from the driving fields. These mechanisms have been considered in many studies for molecular beam [52] and trapped molecular ion Ramsey spectroscopy experiments [48,53].

The scheme phases, wavelengths, and Rabi frequencies can be optimized experimentally despite the use of a racemic sample by using two sequential stages of 3WM with a total of five states, as was similarly demonstrated in Pérez *et al.* [42]. The sign of $\Delta_{\mathrm{PV}}^{\mathrm{vib}}$ can be measured using a small sample with enantiomeric excess. This is a less stringent requirement than using such a sample for the entire experiment. Alternatively, concatenation of other methods to our scheme, such as Coulomb explosion [37], can be used to determine the absolute configuration of the molecules [43]. To our knowledge, measuring $\Delta\phi$ for the fields and comparing the sign of the transition dipole moment components is not reliable in extracting the molecule's absolute configuration [43].

IV. SUMMARY AND OUTLOOK

We have presented a framework to perform PV precision measurement in a racemic sample of chiral molecules that is readily applicable to existing experiments using vibrational spectroscopy [31] as well as pure rotational 3WM [30,46]. The differential scheme benefits from common-mode noise rejection such that statistical uncertainty estimations at the SQL are realistic. The simulations in this work used the $\Delta_{\mathrm{PV}}^{\mathrm{vib}}$ shifts expected in neutral molecule NUHFI since it was previously proposed for a two-level Ramsey spectroscopy experiment [31].

However, our own plan is to realize this method with charged chiral molecules, which can be trapped, facilitating measurements at long coherence times [48]. PV for such charged chiral molecules has been evaluated in a few cases [57,58] and ionization has also been suggested to substantially enhance PV [15].

Indeed, it was recently found that CHDBrI^{+} and $\mathrm{CHCaBrI}^{+}$ exhibit large vibrational PV shifts [19,20]. For example, in CHDBrI^{+}, $2\Delta_{\mathrm{PV}}^{\mathrm{vib}}$ equals $2\pi \times 1.3$ Hz for the C-H stretch mode. For the C-H wag mode the shift is even larger, where $2\Delta_{\mathrm{PV}}^{\mathrm{vib}} = 2\pi \times 1.8$ Hz [19]. Interestingly, for the C-H wag mode, the vibrational radiative lifetime is on the scale of multiple seconds [19], such that the approximate coherence time used in our estimates above are conservative with a lot of room for potential improvement. For $\mathrm{CHCaBrI}^{+}$, $2\Delta_{\mathrm{PV}}^{\mathrm{vib}}$ is as large as $2\pi \times 0.2$ Hz. In Ref. [20], these molecular ion species are proposed for precision spectroscopy, along with details about their quantum state preparation via photoionization and readout by photodissociation.

ACKNOWLEDGMENTS

We thank M. Krüger and Y. Soreq for careful reading of the manuscript and B. Darquié for helpful discussions. Y. S. is thankful for support from the Israel Science Foundation Grant No. 1142/21 and the Council for Higher Education Support Program for Hiring Outstanding Faculty Members in Quantum Science and Technology in Research Universities. This research was partially supported by the Helen Diller Quantum Center at the Technion. E. R. W. acknowledges the support of the Technion Excellence Program for undergraduate students.

APPENDIX: *IN SITU* MAGNETIC FIELD MEASUREMENT

An ambient magnetic field B_a can shift the energies of the three levels involved in our scheme. Such a shift is important to characterize in a precision measurement to estimate systematic uncertainty [56]. Here we show that the embedded simultaneous Ramsey scheme we propose enables an *in situ* measurement of the ambient magnetic field $B = B_a$, and facilitates its zeroing. The capability arises from the different sensitivities of states $|2\rangle$ and $|3\rangle$ to an external magnetic field. Different Landé g factors and Zeeman sublevels m correspond to different magnetic moments $\mu_2 = \mu_B g_2 m_2$ and $\mu_3 = \mu_B g_3 m_3$ for $|2\rangle$ and $|3\rangle$, respectively. Here μ_B is the Bohr magneton. We define $\mu_m = (\mu_B/2)(g_3 m_3 + g_2 m_2)$ and $\mu_\Delta = (\mu_B/2)(g_3 m_3 - g_2 m_2)$ as the mean and difference magnetic sensitivities, such that the magnetic moments of states $|2\rangle$ and $|3\rangle$ are $\mu_{\tilde\Sigma} = \mu_m + \tilde\Sigma \mu_\Delta$, using the $\tilde\Sigma$ switch to distinguish between the two states. The shift in state $|1\rangle$ is not considered since it is common with respect to the two excited states and is the initial state for both enantiomers. The Hamiltonian including the Zeeman shift is

$$\frac{H_{\mathrm{RWA}}^{Z}}{\hbar} = \begin{pmatrix} 0 & \Omega_{\mathrm{P}}(t) & \Omega_{\mathrm{Q}}(t) \\ & \delta - \delta_{\mathrm{S}}/2 + (\mu_m - \mu_\Delta)B + \tilde\kappa \Delta_{\mathrm{PV}}^{\mathrm{vib}} & \tilde\Phi\, \tilde\kappa\, e^{i\pi/2} \Omega_{\mathrm{S}}(t) \\ \mathrm{c.c.} & & \delta + \delta_{\mathrm{S}}/2 + (\mu_m + \mu_\Delta)B + \tilde\kappa \Delta_{\mathrm{PV}}^{\mathrm{vib}} \end{pmatrix}. \tag{A1}$$

To isolate B, we add a switch of the sign of the microwave detuning δ_{S} such that $\delta_{\mathrm{S}} \to \tilde{\mathrm{S}} \delta_{\mathrm{S}}$, where $\tilde{\mathrm{S}} = \pm 1$. To maintain the condition $\delta_{\mathrm{P}} - \delta_{\mathrm{Q}} + \delta_{\mathrm{S}} = 0$ the additional transformation of $\delta_{\mathrm{P}} \to \tilde{\mathrm{S}} \delta_{\mathrm{P}}$ and $\delta_{\mathrm{Q}} \to \tilde{\mathrm{S}} \delta_{\mathrm{Q}}$ must accompany the switch (note that $\delta \to \tilde{\mathrm{S}} \delta$). The frequency of each switch state including the magnetic field is

$$\delta_{\tilde\Phi, \tilde\Sigma, \tilde{\mathrm{S}}} = \tilde{\mathrm{S}} \delta + \tilde\Sigma\, \tilde{\mathrm{S}} \frac{\delta_{\mathrm{S}}}{2} + (\mu_m + \tilde\Sigma \mu_\Delta) B - \tilde\Phi\, \tilde\Sigma\, \Delta_{\mathrm{PV}}^{\mathrm{vib}}. \tag{A2}$$

For a magnetic field $B = 0$ and the case $\tilde{\mathrm{S}} = 1$, Eq. (9) is retrieved. When the new switch $\tilde{\mathrm{S}}$ is added to the two previous switches $\tilde\Sigma$ and $\tilde\Phi$, the total number of frequency channels and linear combinations grows to 2^3. These are given by

$$2\pi \begin{pmatrix} f_0 \\ f_\Phi \\ f_\Sigma \\ f_{\Phi\Sigma} \\ f_{\mathrm{S}} \\ f_{\Phi\mathrm{S}} \\ f_{\Sigma\mathrm{S}} \\ f_{\Phi\Sigma\mathrm{S}} \end{pmatrix} \equiv \frac{1}{8} \begin{pmatrix} + & + & + & + & + & + & + & + \\ + & + & + & + & - & - & - & - \\ + & + & - & - & + & + & - & - \\ + & + & - & - & - & - & + & + \\ + & - & + & - & + & - & + & - \\ + & - & + & - & - & + & - & + \\ + & - & - & + & + & - & - & + \\ + & - & - & + & - & + & + & - \end{pmatrix} \begin{pmatrix} \delta_{\Phi^+,\Sigma^+,\mathrm{S}^+} \\ \delta_{\Phi^+,\Sigma^+,\mathrm{S}^-} \\ \delta_{\Phi^+,\Sigma^-,\mathrm{S}^+} \\ \delta_{\Phi^+,\Sigma^-,\mathrm{S}^-} \\ \delta_{\Phi^-,\Sigma^+,\mathrm{S}^+} \\ \delta_{\Phi^-,\Sigma^+,\mathrm{S}^-} \\ \delta_{\Phi^-,\Sigma^-,\mathrm{S}^+} \\ \delta_{\Phi^-,\Sigma^-,\mathrm{S}^-} \end{pmatrix} = \begin{pmatrix} \mu_m B \\ 0 \\ \mu_\Delta B \\ -\Delta_{\mathrm{PV}}^{\mathrm{vib}} \\ \delta \\ 0 \\ \delta_{\mathrm{S}}/2 \\ 0 \end{pmatrix}. \tag{A3}$$

Importantly, the ambient magnetic field does not affect the $f_{\Phi\Sigma}$ channel, which rejects Zeeman shifts, even if they are state dependent. Moreover, the magnetic field B is measured in a resolved manner since it is the leading term in the f_{Σ} channel, proportional to μ_{Δ} as well as in the f_0 channel, which is proportional to μ_m. This enables the measurement of the average vibrational detuning δ through the f_S channel. Preferably, f_{Σ} and f_0 channels can be used to apply a correction field of opposite sign $B_c = -B_a$ to zero the total magnetic field the molecules experience and prevent other systematic effects it may cause.

The procedure used to null the ambient magnetic fields can be employed to directly monitor and suppress other noise sources to isolate the PV signal by adding the relevant switch to the experiment. This procedure is possible, because the scheme is embedded within the three-state manifold, since the two excited states used for the spectroscopy are likely to have different sensitivities to ambient effects. As discussed in the main text, if Ramsey spectroscopy between a ground and excited vibrational state is applied to a racemic sample, most external effects will cause similar shifts to both enantiomers and preclude their monitoring. While such shifts will likely be suppressed to first order, this is not guaranteed for all effects and thus monitoring them is beneficial.

Note that exciting a single m level in states $|2\rangle$ and $|3\rangle$ under the assumption that these are nearly degenerate is feasible if $|1\rangle$ corresponds to the rotational ground state of the molecule. Alternatively, in a trapped molecular ion experiment where pulse duration can be long, the degeneracy may be lifted with an external magnetic field that is monitored and not suppressed.

[1] C. S. Wu, E. Ambler, R. W. Hayward, D. D. Hoppes, and R. P. Hudson, *Experimental test of parity conservation in beta decay*, Phys. Rev. **105**, 1413 (1957).

[2] T. D. Lee and C. N. Yang, *Question of parity conservation in weak interactions*, Phys. Rev. **104**, 254 (1956).

[3] M. Bouchiat and C. Bouchiat, *I. Parity violation induced by weak neutral currents in atomic physics*, J. Phys. (Paris) **35**, 899 (1974).

[4] M. Bouchiat, J. Guena, L. Hunter, and L. Pottier, *Observation of a parity violation in cesium*, Phys. Lett. B **117**, 358 (1982).

[5] C. S. Wood, S. C. Bennett, D. Cho, B. P. Masterson, J. L. Roberts, C. E. Tanner, and C. E. Wieman, *Measurement of parity nonconservation and an anapole moment in cesium*, Science **275**, 1759 (1997).

[6] C. Wieman and A. Derevianko, *Atomic parity violation and the standard model*, arXiv:1904.00281.

[7] F. Hund, *Zur deutung der molekelspektren. III. Bemerkungen über das schwingungs- und rotationsspektrum bei molekeln mit mehr als zwei kernen*, Z. Phys. **43**, 805 (1927).

[8] M. Quack, *Molecular Parity Violation and chirality: The asymmetry of life and the symmetry violations in physics*, *Quantum Systems in Chemistry and Physics* (Springer, Dordrecht, 2012), pp. 47–76.

[9] V. Letokhov, *On difference of energy levels of left and right molecules due to weak interactions*, Phys. Lett. A **53**, 275 (1975).

[10] M. Quack and J. Stohner, *Influence of parity violating weak nuclear potentials on vibrational and rotational frequencies in chiral molecules*, Phys. Rev. Lett. **84**, 3807 (2000).

[11] Y. Yamagata, *A hypothesis for the asymmetric appearance of biomolecules on earth*, J. Theor. Biol. **11**, 495 (1966).

[12] P. Frank, W. A. Bonner, and R. N. Zare, *On one hand but not the other: The challenge of the origin and survival of homochirality in prebiotic chemistry*, *Chemistry for the 21st Century* (John Wiley & Sons, Ltd, New York, 2000), Chap. 11, pp. 175–208.

[13] M. Quack, *How important is parity violation for molecular and biomolecular chirality?*, Angew. Chem., Int. Ed. **41**, 4618 (2002).

[14] M. Fujiki, J. R. Koe, and S. Amazumi, *Questions of mirror symmetry at the photoexcited and ground states of non-rigid luminophores raised by circularly polarized luminescence and circular dichroism spectroscopy. Part 2: Perylenes, bodipys, molecular scintillators, coumarins, rhodamine B, and DCM*, Symmetry **11**, 363 (2019).

[15] M. Senami and K. Ito, *Asymmetry of electron chirality between enantiomeric pair molecules and the origin of homochirality in nature*, Phys. Rev. A **99**, 012509 (2019).

[16] M. S. Safronova, D. Budker, D. DeMille, Derek F. Jackson Kimball, A. Derevianko, and C. W. Clark, *Search for new physics with atoms and molecules*, Rev. Mod. Phys. **90**, 025008 (2018).

[17] K. Gaul, M. G. Kozlov, T. A. Isaev, and R. Berger, *Chiral molecules as sensitive probes for direct detection of $\mathcal{P}$-odd cosmic fields*, Phys. Rev. Lett. **125**, 123004 (2020).

[18] N. Kuroda, T. Oho, M. Senami, and A. Sunaga, *Enhancement of the parity-violating energy difference of* H_2X_2 *molecules by electronic excitation*, Phys. Rev. A **105**, 012820 (2022).

[19] Eduardus, Y. Shagam, A. Landau, S. Faraji, P. Schwerdtfeger, A. Borschevsky, and L. F. Pašteka, *Large vibrationally induced parity violation effects in* $CHDBrI^+$*—A promising candidate for future experiments*, arXiv:2306.09763.

[20] A. Landau, Eduardus, D. Behar, E. R. Wallach, L. F. Pašteka, S. Faraji, A. Borschevsky, and Y. Shagam, *Chiral molecule candidates for trapped ion spectroscopy by ab initio calculations: From state preparation to parity violation*, J. Chem. Phys. **159**, 114307 (2023).

[21] P. Schwerdtfeger, J. Gierlich, and T. Bollwein, *Large parity-violation effects in heavy-metal-containing chiral compounds*, Angew. Chem., Int. Ed. **42**, 1293 (2003).

[22] P. Schwerdtfeger and R. Bast, *Large parity violation effects in the vibrational spectrum of organometallic compounds*, J. Am. Chem. Soc. **126**, 1652 (2004).

[23] D. Figgen and P. Schwerdtfeger, *Structures, inversion barriers, and parity violation effects in chiral SeO XY molecules* ($X, Y =$ H, *F, Cl, Br, or I*), J. Chem. Phys. **130**, 054306 (2009).

[24] D. Figgen, A. Koers, and P. Schwerdtfeger, *NWHClI: A small and compact chiral molecule with large parity-violation*

effects in the vibrational spectrum, Angew. Chem., Int. Ed. **49**, 2941 (2010).

[25] M. Wormit, M. Olejniczak, A.-L. Deppenmeier, A. Borschevsky, T. Saue, and P. Schwerdtfeger, *Strong enhancement of parity violation effects in chiral uranium compounds*, Phys. Chem. Chem. Phys. **16**, 17043 (2014).

[26] M. Quack, *On the measurement of the parity violating energy difference between enantiomers*, Chem. Phys. Lett. **132**, 147 (1986).

[27] A. Bauder, A. Beil, D. Luckhaus, F. Müller, and M. Quack, *Combined high resolution infrared and microwave study of bromochlorofluoromethane*, J. Chem. Phys. **106**, 7558 (1997).

[28] C. Daussy, T. Marrel, A. Amy-Klein, C. T. Nguyen, C. J. Bordé, and C. Chardonnet, *Limit on the parity nonconserving energy difference between the enantiomers of a chiral molecule by laser spectroscopy*, Phys. Rev. Lett. **83**, 1554 (1999).

[29] C. Stoeffler, B. Darquié, A. Shelkovnikov, C. Daussy, A. Amy-Klein, C. Chardonnet, L. Guy, J. Crassous, T. R. Huet, P. Soulard, and P. Asselin, *High resolution spectroscopy of methyltrioxorhenium: Towards the observation of parity violation in chiral molecules*, Phys. Chem. Chem. Phys. **13**, 854 (2011).

[30] L. Satterthwaite, G. Koumarianou, D. Sorensen, and D. Patterson, *Sub-Hz differential rotational spectroscopy of enantiomers*, Symmetry **14**, 28 (2022).

[31] A. Cournol, M. Manceau, M. Pierens, L. Lecordier, D. B. A. Tran, R. Santagata, B. Argence, A. Goncharov, O. Lopez, M. Abgrall *et al.*, *A new experiment to test parity symmetry in cold chiral molecules using vibrational spectroscopy*, Quantum Electron. **49**, 288 (2019).

[32] J. Eills, J. W. Blanchard, L. Bougas, M. G. Kozlov, A. Pines, and D. Budker, *Measuring molecular parity nonconservation using nuclear-magnetic-resonance spectroscopy*, Phys. Rev. A **96**, 042119 (2017).

[33] B. A. Stickler, M. Diekmann, R. Berger, and D. Wang, *Enantiomer superpositions from matter-wave interference of chiral molecules*, Phys. Rev. X **11**, 031056 (2021).

[34] B. Darquié, C. Stoeffler, A. Shelkovnikov, C. Daussy, A. Amy-Klein, C. Chardonnet, S. Zrig, L. Guy, J. Crassous, P. Soulard, P. Asselin, T. R. Huet, P. Schwerdtfeger, R. Bast, and T. Saue, *Progress toward the first observation of parity violation in chiral molecules by high-resolution laser spectroscopy*, Chirality **22**, 870 (2010).

[35] M. Schnell and J. Küpper, *Tailored molecular samples for precision spectroscopy experiments*, Faraday Discuss. **150**, 33 (2011).

[36] N. Berova, K. Nakanishi, and R. W. Woody, *Circular Dichroism: Principles and Applications* (John Wiley & Sons, New York, 2000).

[37] M. Pitzer, M. Kunitski, A. S. Johnson, T. Jahnke, H. Sann, F. Sturm, L. P. H. Schmidt, H. Schmidt-Böcking, R. Dörner, J. Stohner, J. Kiedrowski, M. Reggelin, S. Marquardt, A. Schießer, R. Berger, and M. S. Schöffler, *Direct determination of absolute molecular stereochemistry in gas phase by Coulomb explosion imaging*, Science **341**, 1096 (2013).

[38] E. Hirota, *Triple resonance for a three-level system of a chiral molecule*, Proc. Jpn. Acad. Ser. B **88**, 120 (2012).

[39] D. Patterson, M. Schnell, and J. M. Doyle, *Enantiomer-specific detection of chiral molecules via microwave spectroscopy*, Nature (London) **497**, 475 (2013).

[40] S. Eibenberger, J. Doyle, and D. Patterson, *Enantiomer-specific state transfer of chiral molecules*, Phys. Rev. Lett. **118**, 123002 (2017).

[41] C. Pérez, A. L. Steber, S. R. Domingos, A. Krin, D. Schmitz, and M. Schnell, *Coherent enantiomer-selective population enrichment using tailored microwave fields*, Angew. Chem., Int. Ed. **56**, 12512 (2017).

[42] C. Pérez, A. L. Steber, A. Krin, and M. Schnell, *State-specific enrichment of chiral conformers with microwave spectroscopy*, J. Phys. Chem. Lett. **9**, 4539 (2018).

[43] S. R. Domingos, C. Pérez, and M. Schnell, *Sensing chirality with rotational spectroscopy*, Annu. Rev. Phys. Chem. **69**, 499 (2018).

[44] M. Leibscher, T. F. Giesen, and C. P. Koch, *Principles of enantio-selective excitation in three-wave mixing spectroscopy of chiral molecules*, J. Chem. Phys. **151**, 014302 (2019).

[45] N. V. Vitanov and M. Drewsen, *Highly efficient detection and separation of chiral molecules through shortcuts to adiabaticity*, Phys. Rev. Lett. **122**, 173202 (2019).

[46] J. H. Lee, J. Bischoff, A. O. Hernandez-Castillo, B. Sartakov, G. Meijer, and S. Eibenberger-Arias, *Quantitative study of enantiomer-specific state transfer*, Phys. Rev. Lett. **128**, 173001 (2022).

[47] M. Leibscher, E. Pozzoli, C. Pérez, M. Schnell, M. Sigalotti, U. Boscain, and C. P. Koch, *Full quantum control of enantiomer-selective state transfer in chiral molecules despite degeneracy*, Commun. Phys. **5**, 110 (2022).

[48] Y. Zhou, Y. Shagam, W. B. Cairncross, K. B. Ng, T. S. Roussy, T. Grogan, K. Boyce, A. Vigil, M. Pettine, T. Zelevinsky, J. Ye, and E. A. Cornell, *Second-scale coherence measured at the quantum projection noise limit with hundreds of molecular ions*, Phys. Rev. Lett. **124**, 053201 (2020).

[49] N. F. Ramsey, *A molecular beam resonance method with separated oscillating fields*, Phys. Rev. **78**, 695 (1950).

[50] B. Argence, B. Chanteau, O. Lopez, D. Nicolodi, M. Abgrall, C. Chardonnet, C. Daussy, B. Darquié, Y. L. Coq, and A. Amy-Klein, *Quantum cascade laser frequency stabilization at the sub-Hz level*, Nat. Photonics **9**, 456 (2015).

[51] J. J. Hudson, D. M. Kara, I. J. Smallman, B. E. Sauer, M. R. Tarbutt, and E. A. Hinds, *Improved measurement of the shape of the electron*, Nature (London) **473**, 493 (2011).

[52] V. Andreev, D. G. Ang, D. DeMille, J. M. Doyle, G. Gabrielse, J. Haefner, N. R. Hutzler, Z. Lasner, C. Meisenhelder, B. R. O'Leary, C. D. Panda, A. D. West, E. P. West, and X. Wu, *Improved limit on the electric dipole moment of the electron*, Nature (London) **562**, 355 (2018).

[53] T. S. Roussy, L. Caldwell, T. Wright, W. B. Cairncross, Y. Shagam, K. B. Ng, N. Schlossberger, S. Y. Park, A. Wang, J. Ye, and E. A. Cornell, *An improved bound on the electron's electric dipole moment*, Science **381**, 46 (2023).

[54] L. Caldwell, T. S. Roussy, T. Wright, W. B. Cairncross, Y. Shagam, K. B. Ng, N. Schlossberger, S. Y. Park, A. Wang, J. Ye, and E. A. Cornell, *Systematic and statistical uncertainty*

evaluation of the HfF^+ *electron electric dipole moment experiment*, Phys. Rev. A **108**, 012804 (2023).

[55] A. T. J. B. Eppink and D. H. Parker, *Velocity map imaging of ions and electrons using electrostatic lenses: Application in photoelectron and photofragment ion imaging of molecular oxygen*, Rev. Sci. Instrum. **68**, 3477 (1997).

[56] X. Wu, Z. Han, J. Chow, D. G. Ang, C. Meisenhelder, C. D. Panda, E. P. West, G. Gabrielse, J. M. Doyle, and D. DeMille, *The metastable* $Q^3\Delta_2$ *state of ThO: A new resource for the ACME electron EDM search*, New J. Phys. **22**, 023013 (2020).

[57] M. Gottselig, M. Quack, J. Stohner, and M. Willeke, *Mode-selective stereomutation tunneling and parity violation in* HOClH^+ *and* $\mathrm{H_2Te_2}$ *isotopomers*, Int. J. Mass Spectrom. **233**, 373 (2004).

[58] J. Stohner, *Parity violating effects in the molecular anion* CBrClF^-, Int. J. Mass Spectrom. **233**, 385 (2004).